

THE COMPOSITION OF MASSIVE SULFIDE DEPOSITS FROM THE SEDIMENT-COVERED FLOOR OF ESCANABA TROUGH, GORDA RIDGE: IMPLICATIONS FOR DEPOSITIONAL PROCESSES

RANDOLPH A. KOSKI

U.S. Geological Survey, MS 999, 345 Middlefield Road, Menlo Park, California 94025, U.S.A.

WAYNE C. SHANKS, III

U.S. Geological Survey, MS 954, National Center, Reston, Virginia 22092, U.S.A.

WENDY A. BOHRSON* AND ROBERT L. OSCARSON

U.S. Geological Survey, MS 999, 345 Middlefield Road, Menlo Park, California 94025, U.S.A.

ABSTRACT

Massive sulfide deposits with two distinct compositions are spatially related to volcanic edifices that penetrate up to 500 m of turbiditic sediment in Escanaba Trough (ET), southern Gorda Ridge. Constructional sulfide mounds and chimneys occur on the peripheries of steep-sided, sediment-capped hills at the southern or SESCO site near 40°45' N latitude and the northern or NESCA site near 41°N latitude, and on the stepfaulted flank of a broad volcanic hill at the NESCA site. Unzoned pyrrhotite-rich massive sulfides dredged from mounds in the SESCO and NESCA sites have low amounts of Zn, Pb, Cd, Ba, and Ag, and thin (<2 cm) barite crusts. Grain-size variations mark the locations of myriad fluid channelways through the sulfide mounds. Zoned polymetallic (Fe-Zn-Pb-Cu-As-Ag-Sb) sulfides from the NESCA site are pieces of a sulfide structure with a large central conduit. In the polymetallic sulfide structure, the inner-wall (sphalerite + isocubanite) and middle-wall (pyrrhotite + sphalerite + isocubanite + arsenopyrite + löllingite) assemblages crystallized inward toward hydrothermal fluid, whereas the outer-wall assemblage (sphalerite + galena + pyrrhotite + barite + boulangérite + tetrahedrite + acanthite?) grew outward along the mixing interface between hydrothermal fluid and seawater. The mineralogy, metal content, sulfur isotope composition, and hydrocarbon content of massive sulfides from ET reflect the extensive interaction between underlying turbiditic sediment and hydrothermal fluid. Pyrrhotite-rich sulfide mounds are inferred to have formed under gentle temperature and chemical gradients related to diffuse, low-velocity flow through disrupted sediment near the sediment-capped hills. The telescoped zoning in the polymetallic sulfide structure apparently developed in response to steep temperature and chemical gradients at a site of focused high-velocity discharge, possibly a fault crosscutting a sequence of semilithified turbidites.

Keywords: massive sulfide, Escanaba Trough, Gorda Ridge, pyrrhotite-rich, polymetallic, turbidite, fluid-sediment interaction.

SOMMAIRE

Deux genres de gisements de sulfures massifs, distincts dans leur composition, sont associés aux édifices volcaniques qui pénètrent jusqu'à 500 m de sédiments turbiditiques dans le bassin d'Escanaba, dans le secteur sud de la crête de Gorda. Des amoncèlements de sulfures et des cheminées sont situés à la périphérie des pics recouverts de sédiments aux sites dits SESCO, au sud, près de 40°45' N, et NESCA, au nord, près de 41°N, aussi bien que dans le flanc faillé d'une large colline volcanique au site NESCA. Des échantillons homogènes de sulfures massifs riches en pyrrhotine, dragués près des amoncèlements des sites SESCO et NESCA, sont pauvres en Zn, Pb, Cd, Ba et Ag, et ne possèdent qu'une mince gaine de barytine (< 2 cm). Des variations granulométriques indiquent la location d'une myriade de conduits hydrothermaux à travers les amoncèlements hydrothermaux. Les sulfures zonés polymétalliques (Fe-Zn-Pb-Cu-As-Ag-Sb) du site NESCA sont des fragments d'une cheminée ayant un conduit central imposant. Les assemblages de la paroi interne (sphalérite + isocubanite) et du secteur intermédiaire (pyrrhotine + sphalérite + isocubanite + arsenopyrite + löllingite) se sont formés vers l'intérieur en contact avec le fluide hydrothermal, tandis que l'assemblage de la paroi externe (sphalérite + galène + pyrrhotine + barytine + boulangérite + tétraédrite + acanthite?) s'est formé vers l'extérieur, dans la zone de mélange impliquant le fluide hydrothermal et l'eau de mer. La minéralogie, le contenu des métaux, la composition isotopique du soufre, et le contenu en hydrocarbures des sulfures massifs du bassin d'Escanaba résulteraient d'une interaction importante entre les turbidites sous-jacentes et le fluide hydrothermal. Les amoncèlements riches en pyrrhotine se seraient formés à des températures plus faibles le long de gradients chimiques régis par un flux plus lent et plus diffus à travers les sédiments, près des pics recouverts. La zonation serrée dans la structure à sulfures polymétalliques aurait une explication dans l'existence de gradients thermiques et chimiques importants aux sites de décharge à débit élevé, possiblement le long d'une faille recoupant la séquence de turbidites semi-consolidées.

(Traduit par la Rédaction)

* Present address: Department of Earth and Space Sciences, University of California, Los Angeles, California 90024, U.S.A.

Mots-clés: sulfures massifs, bassin d'Escanaba, crête de Gorda, enrichissement en pyrrhotine, polymétallique, turbidite, interaction fluide-sédiment.

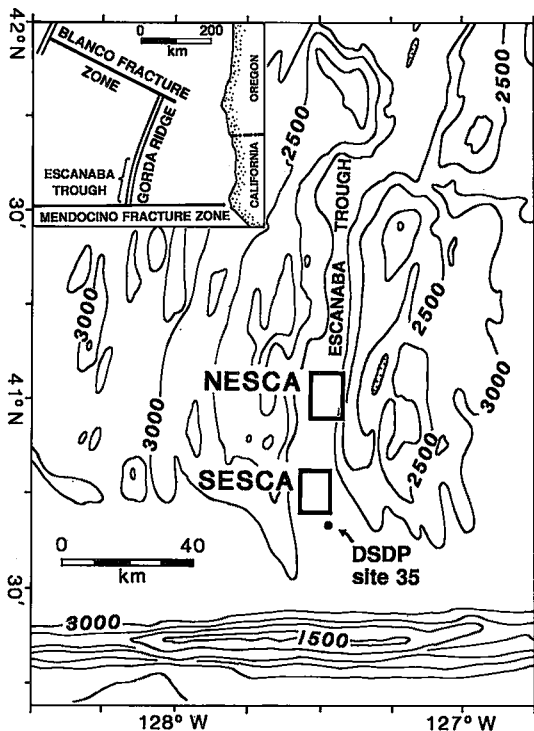


FIG. 1. Location and regional bathymetry of Gorda Ridge and Escanaba Trough. The SESCA and NESCA sites are shown in greater detail in Figures 3a and b. Contour interval is 500 m.

INTRODUCTION

Massive sulfide deposits at sediment-free spreading axes in the eastern Pacific are the end products of geothermal and geochemical processes in the seawater–basalt system. Direct evidence for the interaction between hydrothermal fluid of seawater origin and mid-ocean ridge basalt (MORB) includes: i) the high Fe, Zn, and Cu, and low Pb contents of the massive sulfide deposits (Hékinian *et al.* 1980, Bischoff *et al.* 1983, Hékinian & Fouquet 1985, Bäcker & Lange 1987) and vent fluids (Von Damm *et al.* 1985a, Von Damm & Bischoff 1987); ii) the MORB-like Pb isotope ratios of sulfides (Brevart *et al.* 1981, Vidal & Clauer 1981, LeHuray *et al.* 1988) and fluids (Chen *et al.* 1986); and iii) the predominance of basaltic sulfur in sulfide minerals as indicated by S isotope ratios (Styrt *et al.* 1981, Arnold & Sheppard 1981).

At sediment-covered ridge axes, sulfide deposits result from reactions in the seawater–basalt–sediment system; reactions are further complicated by chemical heterogeneity of the sediment. For example, the interaction between hydrothermal fluid and organic-rich mud turbidite at Guaymas Basin, Gulf of

California, is indicated by the base metal-poor nature of the sulfide deposits (Lonsdale *et al.* 1980, Koski *et al.* 1985, Peter 1986) and vent fluids (Von Damm *et al.* 1985b), the radiogenic Pb isotope ratios of massive sulfides (LeHuray *et al.* 1988) and hydrothermal fluid (Chen *et al.* 1986), and the occurrence of thermogenic petroleum with the sulfides (Simoneit & Lonsdale 1982, Simoneit 1985). Other evidence, including dissolved silica (Von Damm *et al.* 1985b) and ^3He (Lupton 1983) in the vent fluids, and S isotope ratios of sulfide minerals (Shanks & Niemitz 1982, Koski *et al.* 1985, Peter 1986), indicates that fluids in Guaymas Basin have circulated below the sediment cover and reacted with basaltic basement.

This paper presents the results of petrographic and geochemical investigations of sulfide samples dredged in 1986 from Escanaba Trough, the sediment-covered southern end of Gorda Ridge (Fig. 1). The data allow us to make inferences about the interaction between hydrothermal fluids and sediment in Escanaba Trough, and to develop preliminary models for deposition of massive sulfide on a sediment-covered spreading axis.

GEOLOGIC SETTING OF SULFIDE DEPOSITS

Gorda Ridge, a 300-km-long spreading axis in the northeast Pacific Ocean, is bounded to the north by the Blanco Fracture Zone and to the south by the Mendocino Fracture Zone (Fig. 1). The southern third of Gorda Ridge, referred to as Escanaba Trough (ET), is spreading at the relatively slow rate of 2.3 cm/yr (Atwater & Mudie 1973, Riddihough 1980). ET has a morphology similar to that of the Mid-Atlantic Ridge: a deep axial valley at a water depth of about 3200 m is flanked by ridges that rise to water depths of 1500–2000 m. The segment of ET between 41°15' N latitude and the Mendocino Fracture Zone is buried by up to 500 m of turbidite sediment derived from the continental margin of North America, 300 km to the east (Vallier *et al.* 1973, Karlin & Lyle 1986).

Single-channel seismic reflection surveys over ET have revealed a series of volcanic centers spaced at intervals of 15 to 20 km within the axial valley (Morton *et al.* 1987a). These volcanic centers form broad edifices, 3 to 6 km across, that extend upward from the volcanic basement and breach and locally uplift the sediment cover (Fig. 2). Sulfide deposits are associated with the two largest volcanic edifices centered at approximately 40°45' N and 41°00' N latitude, the SESCA and NESCA sites, respectively (Fig. 1).

At the SESCA site (Fig. 3a), sulfide deposits are spatially related to three flat-topped hills about 100 m high and 1 km across that rise above the broad high of the volcanic center. Echo-sounding records across these hills indicate that they are steep-sided domes capped by sediment (Fig. 4). The domes seem

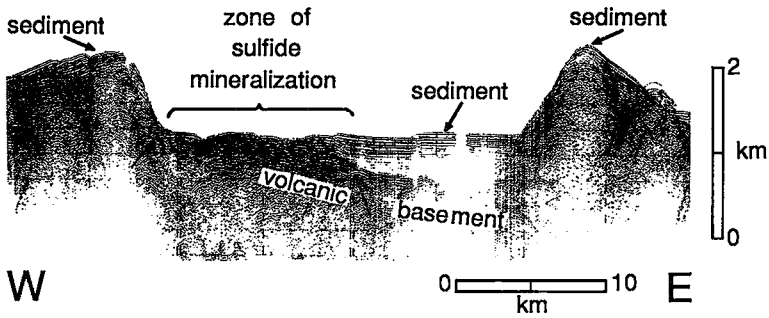


FIG. 2. Single-channel seismic-reflection profile across Escanaba Trough at $40^{\circ}45'$ N latitude (SESCA site). A volcanic edifice rises through turbiditic sediment west of the valley axis. Axis-parallel faults have displaced the sediment east of the volcanic edifice. Vertical exaggeration is $6.4\times$.

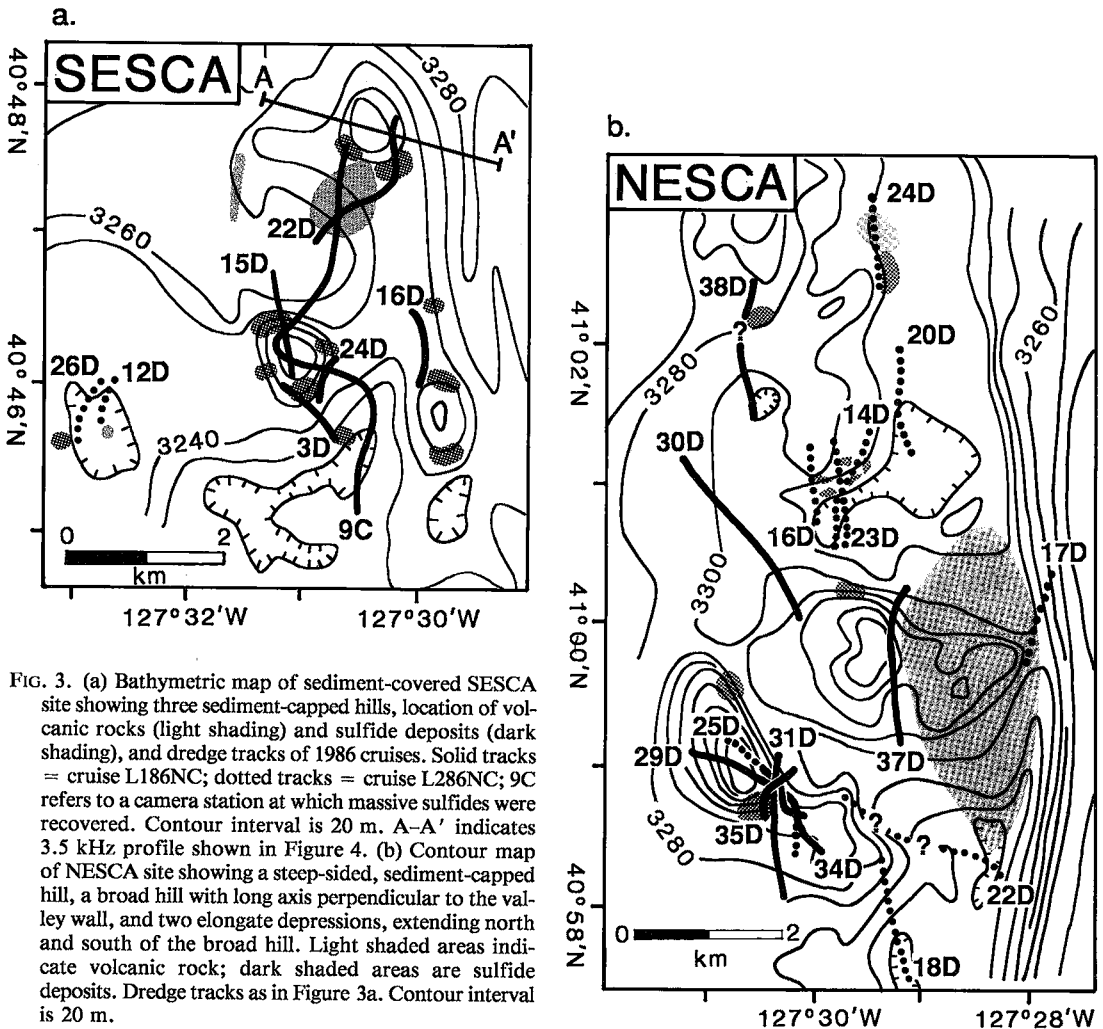


FIG. 3. (a) Bathymetric map of sediment-covered SESCO site showing three sediment-capped hills, location of volcanic rocks (light shading) and sulfide deposits (dark shading), and dredge tracks of 1986 cruises. Solid tracks = cruise L186NC; dotted tracks = cruise L286NC; 9C refers to a camera station at which massive sulfides were recovered. Contour interval is 20 m. A-A' indicates 3.5 kHz profile shown in Figure 4. (b) Contour map of NESCA site showing a steep-sided, sediment-capped hill, a broad hill with long axis perpendicular to the valley wall, and two elongate depressions, extending north and south of the broad hill. Light shaded areas indicate volcanic rock; dark shaded areas are sulfide deposits. Dredge tracks as in Figure 3a. Contour interval is 20 m.

to be sediment blocks uplifted and perhaps cored by igneous intrusions. Deep-tow photographic surveys and submersible observations show that lava flows are exposed between the two northern hills (Fig. 3a). Massive sulfide deposits (Fig. 5a) are constructional mounds that form semi-continuous outcrops as much as 100 m in length and 5 m in height along the margins of the hills (Holmes & Zierenberg 1988). The mounds are topped by a few eroded chimneys (Fig. 5b) and are surrounded by aprons of sulfide talus.

The NESCA site (Fig. 3b) is characterized by a steep-sided, sediment-capped hill to the southwest and by a broader, east-west-trending central hill covered in part by pillow-basalt flows. Massive sulfide deposits as much as 30 m thick occur along the step-faulted, sediment-covered northern flank of this volcanic hill (Holmes & Zierenberg 1988). A north-trending basin north of the volcanic hill may represent a lava lake with a thin sediment cover (Morton *et al.* 1987b). The topographically complex, sediment-covered ridge west of this basin displays numerous channels and craters, a few meters in depth and several tens of meters in width, that may have formed during collapse of underlying lava flows (Holmes & Zierenberg 1988). Sulfide crusts and small chimneys are associated with the channels along the eastern slope of the ridge. Although high heat-flow values and low-level seismicity have been recorded from the area of the sulfide deposits (Abbott *et al.* 1986, Bibee 1986), no active hydrothermal venting has been observed.

SAMPLING AND ANALYTICAL TECHNIQUES

During a 1985 cruise of the USGS research vessel *S.P. Lee* (Morton *et al.* 1987a), 4.5 kg of massive sulfide were dredged (L6-32D) from the SESCO site.

Subsequent cruises in 1986 dredged an additional 43 kg of sulfide from SESCO and 19.5 kg from NESCA. Preliminary descriptions of these samples are reported in Morton *et al.* (1987a), Koski *et al.* (1987), and Benninger & Koski (1987). In the present study, the sulfides recovered in 1986 were investigated using standard incident-light microscopy, scanning-electron-microscopy (SEM), and for quantitative analysis, electron-microprobe (EM) techniques. The composition of small (<5 μm) mineral grains was determined by backscattered electron (BSE) imaging and a semi-quantitative energy-dispersion X-ray analyzer (EDX) attached to a SEM.

Chemical analyses of sulfide- and sulfate-rich samples were obtained by quantitative DC-arc optical emission spectroscopy (Fe, Cu, Zn, Pb, Au, Bi, Cd, Sb, Se, Hg), semiquantitative emission spectroscopy (Ag, As, Ba, Mn, Sn), and LECO* analyzer for total S. Arsenic greater than 0.2 wt% was analyzed by ICP emission spectroscopy. Organic carbon was determined by the difference between carbonate carbon determined by a coulometric technique and total carbon determined by a LECO analyzer. (* Use of tradenames is for descriptive purposes only and does not imply endorsement by the U.S. Geological Survey).

The compositions of Fe-As-S sulfides and a Pb-Sb sulfosalt were determined by wavelength-dispersion analysis with an ARL model SEMQ electron microprobe. The standards used were: pyrrhotite (Fe, S), synthetic NiAs (As), Zn metal (Zn), synthetic CoS (Co) and NiS (Ni), and diaphorite (Sb, Pb, Ag, S). Counting times were at least 60 seconds. Raw analytical data were reduced on-line with the Bence-Albee program modified by Albee & Ray (1970).

For sulfur isotope analyses, pyrrhotite and marcasite concentrates were hand-picked from

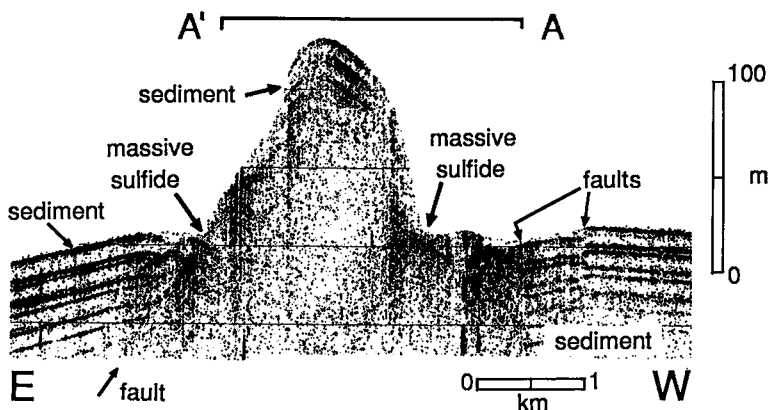


FIG. 4. A 3.5 kHz profile across the northernmost of the 100-m-high, steep-sided hills at the SESCO site. The tilted sediment cap and disrupted sediment near the base may be the result of uplift during volcanic intrusion. Massive sulfide deposits occur above the disrupted zone at base of hill. Vertical exaggeration is 18 \times .

pyrrhotite-rich massive sulfide samples. Sulfate-bearing samples were digested in 1N HCl to remove sulfate. Sulfur fractions were obtained by a series of sequential chemical extractions. Pyrrhotite and any associated sphalerite were dissolved in 6N HCl at 60°C. The resulting H₂S was purged with N₂ gas into a AgNO₃ trap where Ag₂S was quantitatively precipitated. Marcasite-rich fractions were treated similarly, or sequentially by adding CrCl₂ to the 6N HCl solution at 85°C (Canfield *et al.* 1986). The Ag₂S precipitates were combusted with Cu₂O at 1050°C to produce SO₂, which was purified by vacuum distillation. The δ³⁴S values were determined on a 6-inch (15.2 cm) 60° Nuclide Corporation mass spectrometer. The δ³⁴S values are standardized to the Cañon Diablo troilite (CDT) using the McMaster University reference standards of Rees (1978). Analytical precision based on multiple analyses of sulfide standard NBS-123 is ±0.14 per mil (1 standard deviation).

MINERALOGY OF SULFIDE SAMPLES

The massive sulfide samples are subdivided into two types on the basis of composition and texture: pyrrhotite-rich sulfide and polymetallic sulfide. The mineralogy and relative mineral abundances in each sulfide type are given in Table 1.

Pyrrhotite-rich sulfides

Eighty percent of the massive sulfide samples are porous, chemically homogeneous aggregates of hexagonal pyrrhotite with minor interstitial sphalerite and Cu-Fe sulfides (Fig. 6a). Interpenetrating pyrrhotite crystals form a boxwork texture with 10 to 15% porosity. In many samples, vuggy zones with randomly oriented coarse-grained pyrrhotite plates are enclosed by euhedral pyrrhotite with radial orientation; these zones represent fossil fluid channelways. Pyrrhotite-rich massive sulfides with boxwork texture have also been recovered from other sediment-covered spreading axes at Guaymas Basin (Koski *et al.* 1985) and Middle Valley, northern Juan de Fuca Ridge (Davis *et al.* 1987).

Marcasite is abundant in some samples as a partial to complete pseudomorphic replacement of pyrrhotite. Marcasite-rich samples are friable and have one or more Fe-oxide-encrusted surfaces. Less altered pyrrhotite is partly replaced by a strongly anisotropic Fe sulfide phase along cracks and grain margins (Fig. 7a). SEM microanalysis indicates that this phase has a composition with a slightly lower Fe/S ratio than pyrrhotite. Optically, this material resembles the "intermediate product" of pyrrhotite alteration described by Einaudi (1971). The dark zones between original pyrrhotite and the secondary Fe sulfide (Fig. 7a) may be void space created by the

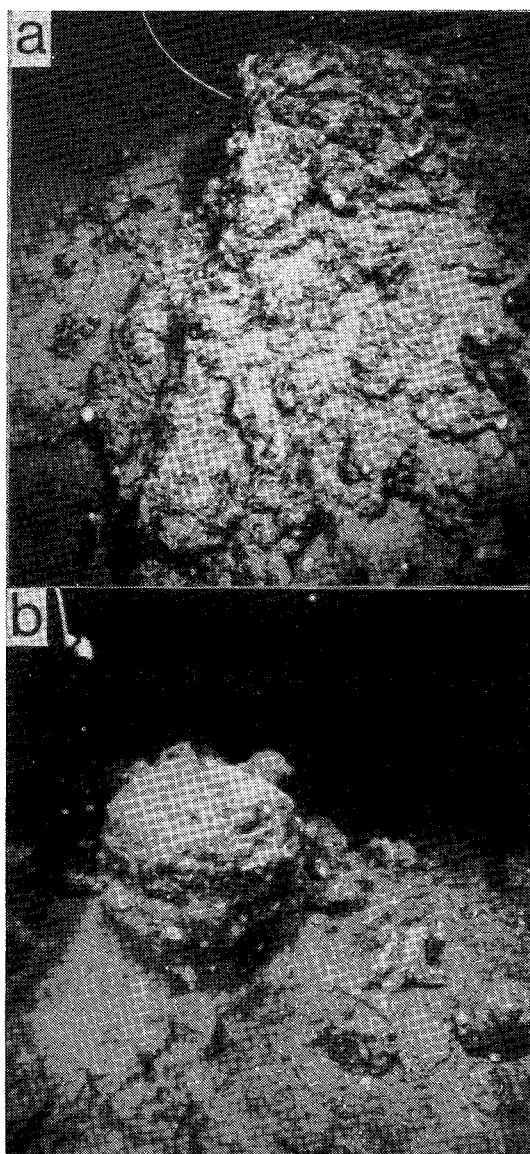


FIG. 5. (a) Massive sulfide mound at base of sediment-capped hill at the SESCO site. The rubbly, eroded surface and absence of vent-specific organisms indicate that the vent site is inactive. The high part of the mound is approximately 3 m across. (b) The eroded base of a sulfide chimney, approximately 0.3 m wide, on rubbly sulfide mound at SESCO site.

volume decrease which accompanies the pyrrhotite → marcasite replacement reaction (Murowchick & Barnes 1984, 1986). Where alteration is more advanced, the zones of secondary Fe sulfide widen and coalesce around cores of pyrrhotite. The final alteration product is a pseudomorphic aggregate of

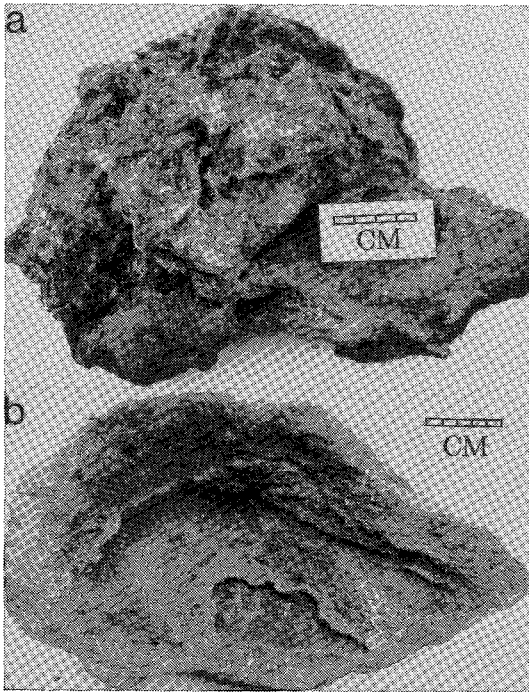


FIG. 6. (a) Fragment of pyrrhotite-rich massive sulfides from dredge L1-24D, SESCO site. (b) Bowl-shaped polymetallic massive sulfide sample from dredge L2-14D, NESCA site.

marcasite, or marcasite + Fe oxide. Extensive alteration of pyrrhotite by marcasite has also been described in sulfide samples from Middle Valley (Davis *et al.* 1987).

Pyrite is the least abundant Fe sulfide phase, but is concentrated along the edges of a few sulfide samples as anhedral-granular aggregates, framboids, and colloform growth forms.

Anhedral to subhedral blebs of Cu-Fe sulfide, generally intergrown with or rimmed by sphalerite, occur in the interstices among pyrrhotite grains which are also partly replaced. Identical textures and parageneses have been described in massive sulfide samples from Guaymas Basin (Koski *et al.* 1985, Peter 1986). The Cu-Fe sulfide phases are isocubanite and chalcopyrite; commonly, isocubanite displays oriented, spindle-shaped lamellae and narrow rims of chalcopyrite (Fig. 7b). Minor amounts of covellite and digenite occur as fine-grained scaly masses on the fringes of Cu-Fe sulfide grains, and as inclusions in marcasite derived from the alteration of pyrrhotite. The covellite and digenite are most abundant where such alteration is advanced.

Löllingite (FeAs_2) occurs in layers of fine-grained wedge-shaped crystals that appear superimposed on coarser pyrrhotite (Fig. 7c). Löllingite in one sample is concentrated within radially oriented pyrrhotite that surrounds a fossil fluid channelway. Löllingite grains typically contain minute ($<2\mu\text{m}$) anhedral inclusions of native bismuth (Fig. 7c). An EDX analysis indicates that such native bismuth grains contain about 10 wt.% Sb.

TABLE 1. MINERALOGY OF MASSIVE SULFIDE SAMPLES

	Pyrrhotite-rich	Polymetallic
Major:	pyrrhotite, (marcasite), (talc), (barite)	sphalerite, pyrrhotite, galena, isocubanite,
Minor:	isocubanite, chalcopyrite, sphalerite, barite	arsenopyrite, barite
Trace:	pyrite, löllingite, galena, native bismuth, covellite, digenite, amorphous silica, talc	löllingite, tetrahedrite, boulangierite, native bismuth, Ag sulfide (acanthite?)

(): marcasite, talc, and barite are major phases in some pyrrhotite-rich samples.

Many pyrrhotite-rich samples have 1- to 2-cm-thick crusts composed of drusy barite and sulfide. Barite tablets up to 2.5 mm in length generally occur in radiating clusters or dendrites that extend outward from the sulfide substrate. The barite crystals are typically infilled and overgrown by colloform sphalerite followed by anhedral galena (Fig. 7d). Framboidal pyrite and colloform to granular marcasite and pyrite are also intergrown with barite. Interstitial Cu-Fe sulfide, overgrown by sphalerite, is concentrated adjacent to the contact between barite and pyrrhotite-rich substrate. The barite crusts also contain swirly layers of amorphous Fe oxide and silica.

Two dredges from the SESCO site recovered numerous slabby fragments of pyrrhotite-rich sulfides with thick (5 to 10 cm) encrustations of massive talc containing minor intergrown chlorite and pyrrhotite. Cavities and interstices in the pyrrhotite-rich sulfides are lined or filled with talc. The morphology and composition of the slabby pyrrhotite-talc samples suggest that they formed as encrustations on the sediment surface. Ledges of massive talc and pyrrhotite have been observed and sampled on the floor of the Guaymas Basin in the Gulf of California (Lonsdale *et al.* 1980).

Polymetallic sulfides

A single dredge haul at the NESCA site (L2-14D) recovered 12 kg of dark grey, zoned massive sulfides. A large bowl-shaped fragment (Fig. 6b) appears to be part of a sulfide vent structure which had a large central conduit. A cross-section through this wall can be divided into inner, middle and outer zones on the basis of mineralogical and textural characteristics (Fig. 8). From inner to outer wall, grain size decreases and textures change from inward-directed and euhedral-granular to outward-directed and dendritic or colloform.

Polymetallic sulfides

The concave inner zone of the wall is composed of a coarse-grained assemblage of isocubanite + sphalerite (Fig. 9a). Euhedral to subhedral sphalerite encloses feathery and skeletal cores of isocubanite

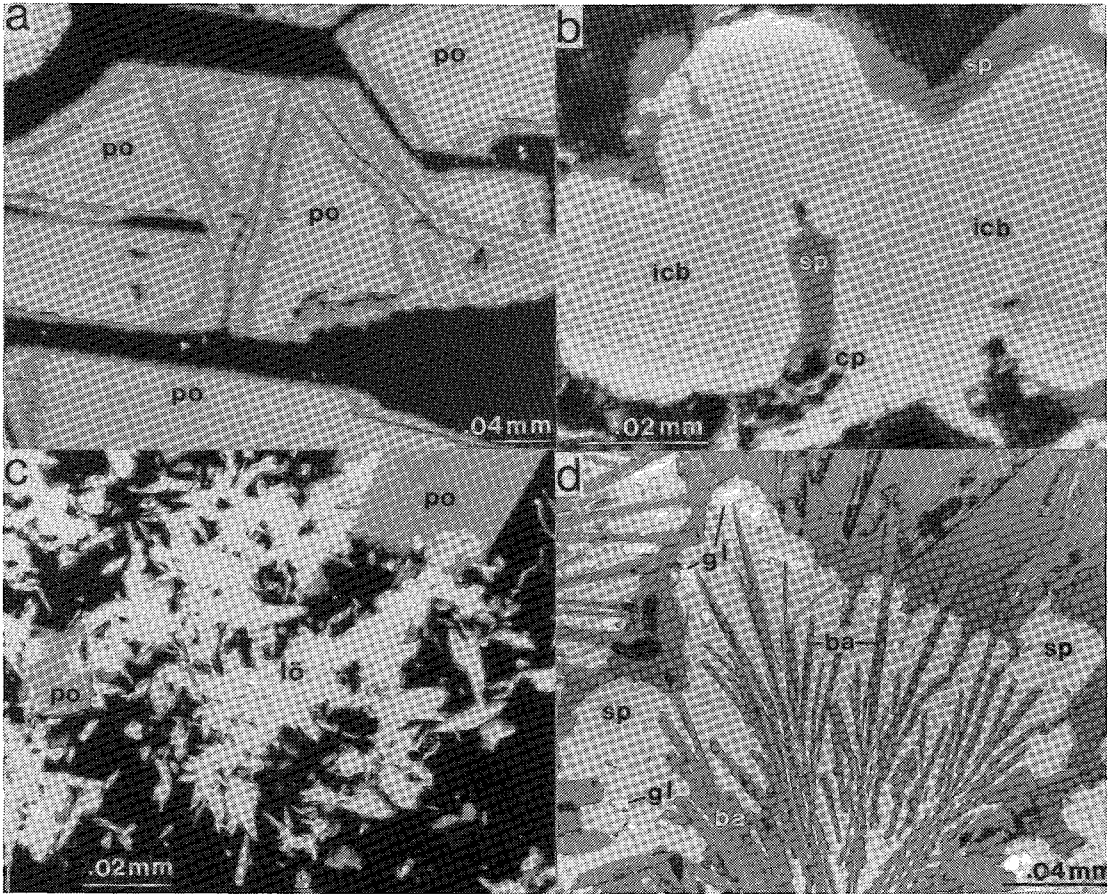


FIG. 7. Pyrrhotite-rich massive sulfides. (a) BSE image of pyrrhotite grains (po) altered to intermediate Fe sulfide phase along grain margins and cracks. (b) Reflected-light photomicrograph of Cu-Fe sulfide grain in which isocubanite (icb) displays oriented spindly lamellae and rims of chalcopyrite (cp). The entire grain is overgrown by sphalerite (sp). (c) BSE image showing fine-grained aggregate of wedge-shaped löllingite crystals (lö) superimposed on pyrrhotite plates (po). Small white specks in löllingite are inclusions of native bismuth. (d) Reflected-light photomicrograph showing radiating barite needles (ba) overgrown by dendritic and colloform sphalerite (sp) and anhedral-granular galena (gl).

that grade outward into finely disseminated Cu-Fe sulfide blebs. This texture resembles the “chalcopyrite disease” of Barton (1978) and the “watermelon texture” of Barton & Bethke (1987).

The thicker middle wall contains pyrrhotite-rich layers alternating with layers of granular sphalerite and isocubanite which resemble the inner-wall assemblage. Platy pyrrhotite grains are oriented radially, and decrease in size toward the outer wall. Sphalerite and isocubanite occupy interstices between pyrrhotite plates, and coarse-grained arsenopyrite has replaced pyrrhotite along the boundary with the inner

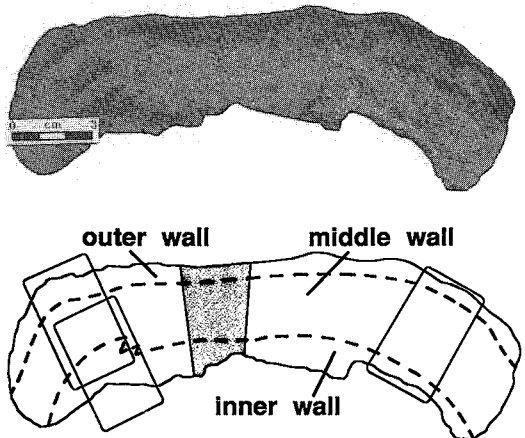


FIG. 8. Cross-section of polymetallic sulfide wall paired with sketch showing inner, middle, and outer wall. The sketch gives locations of polished thin sections (open rectangles) and area sampled for chemical analyses (shaded region).

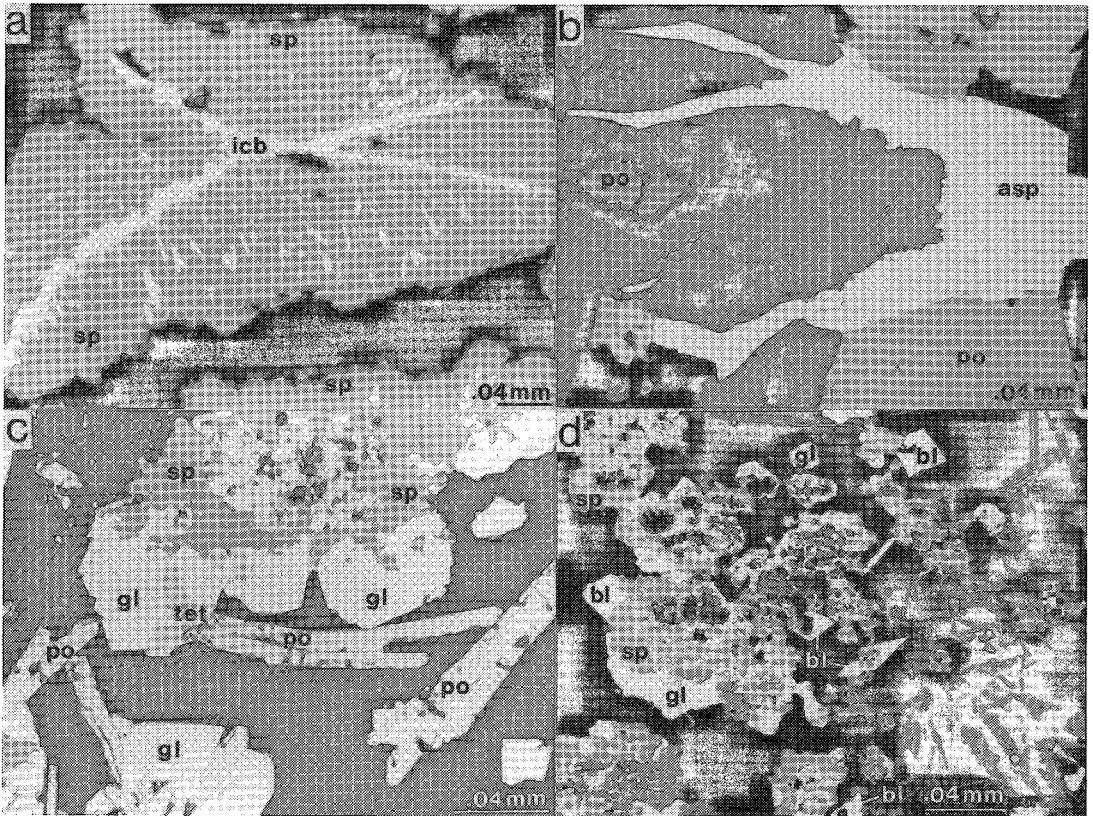


FIG. 9. Polymetallic massive sulfide. (a) Reflected-light photomicrograph of sphalerite grain (sp) with skeletal replacement by isocubanite (icb) from inner wall of polymetallic sulfide structure. (b) BSE image of pyrrhotite (po) replaced by irregular arsenopyrite (asp) grain in middle wall near contact with inner wall. Pyrrhotite is also partly altered to secondary Fe sulfide and Fe oxide (non-reflective area). (c) Reflected-light photomicrograph of fine-grained pyrrhotite (po) + sphalerite (sp) + galena (gl) + tetrahedrite (tet) in outer wall. (d) BSE image of boulangerite (bl) associated with fine-grained sphalerite (sp) and galena (gl) in outer wall.

wall (Fig. 9b). Each pyrrhotite layer in the middle wall provided a substrate for inward growth of the adjacent sphalerite + isocubanite layer, and is partly replaced by these minerals. Within the outer half of the middle wall, fine-grained arsenopyrite with inclusions of native bismuth is concentrated in narrow layers. Galena, absent in the inner wall, becomes increasingly abundant toward the outer part of the middle wall. The outermost pyrrhotite layer within the middle wall displays replacement by marcasite along cracks.

The thin, friable outer wall has a "primitive" texture resulting from the outward growth of dendritic, colloform, and fine-grained subhedral sphalerite. Galena is common both as inclusions within sphalerite and as marginal replacements and overgrowths of sphalerite dendrites. In the inner part of this zone, pyrrhotite occurs as fine-grained aggregates of stubby plates; in the outer part, pyrrhotite forms fragile boxworks of small thin platelets between sphalerite masses. Tetrahedrite is inter-

grown with galena on the surface of sphalerite dendrites (Fig. 9c), and an Ag sulfide phase, possibly acanthite, occurs as clusters of 1- μ m inclusions in sphalerite.

Slender prismatic crystals of a Pb-Sb sulfosalt are scattered between sphalerite dendrites in the outer wall (Fig. 9d). EM analyses (Table 2) show that in

TABLE 2. MICROPROBE DATA FOR Pb-Sb SULFOSALT IN SAMPLE L2-14D-1

	Average for 10 analyses	Analysis with highest Pb, lowest Sb	Analysis with lowest Pb, highest Sb
Weight Percent			
S	18.7	18.6	19.6
Sb	25.6	22.1	27.5
Pb	52.9	56.7	50.9
Zn	1.93	1.65	1.98
As	0.20	0.19	0.20
Ag	0.11	0.03	0.01
Total	99.4	99.2	100.2

Microprobe analyses by R. Koski and W. Bohrsen

addition to Pb, Sb, and S, this phase contains about 2 wt.% Zn and traces of Ag and As. PbS/Sb₂S₃ ratios of 2.5 to 3.3 correspond to the mineral formulas (Pb,Zn)₅Sb₄S₁₁ and (Pb,Zn)₁₀Sb₆S₁₉. The former corresponds to the formula for boulangerite. Although Ag is known to occur in lead sulfantimonides (Jambor 1967), a zinc-bearing variety of boulangerite has not been characterized. Hannington *et al.* (1986) recently identified Pb-As-Sb-Ag sulfosalts in low-temperature zones of sulfide mounds and spires from Axial Seamount (Juan de Fuca Ridge) and the southern Explorer Ridge.

Sulfide in sediment

Several sediment samples containing sulfides as massive, interstitial, fracture-controlled, and disseminated mineralization have been dredged from ET. Sandy siltstone dredged from the SESCOA site in 1985 contains layers of pyrrhotite-rich sulfides, as well as asphaltic hydrocarbon (Kvenvolden *et al.* 1986). In several 1986 dredge samples, pyrrhotite-rich sulfides enclose angular clasts of altered siltstone and mudstone. The fine-grained component of the sediment clasts has been altered to talc and chlorite, but detrital quartz, plagioclase, pyroxene, and muscovite grains are preserved. A sample of indurated, coarse sand from the NESCA site (L2-14D-6) is cemented by the polymetallic assemblage galena + sphalerite + pyrrhotite + löllingite, and is saturated with petroleum. Coarse-grained (0.3 mm) euhedral pyrite lines fractures in indurated sediment recovered in dredge L1-3D from SESCOA.

BULK CHEMISTRY

Sulfide and sulfate samples

Bulk chemical analyses for 5 samples of pyrrhotite-rich massive sulfides, a barite crust, two samples of polymetallic massive sulfides, and a sulfide-rich sedi-

ment are given in Table 3. Additional chemical data are in Benninger & Koski (1987). In general, pyrrhotite-rich massive sulfides are characterized by moderate Cu (~1 wt.%) and low Pb, Zn, Cd, Ba, and Ag contents compared to pyrite-bearing massive sulfides from sediment-free spreading axes (*cf.* Bischoff *et al.* 1983). The low combined ore-metal (Cu + Zn + Pb + Ag) content is also characteristic of pyrrhotite-rich samples from Guaymas Basin (Koski *et al.* 1985, Peter 1986) and Middle Valley (Davis *et al.* 1987); the Escanaba samples have, however, higher As, Bi, and Sn. Variation in the Fe/S ratio of pyrrhotite-rich samples largely reflects the degree of pyrrhotite alteration to marcasite. The high C content (5.6 wt.%) of dredge sample L6-32D-2 reflects the presence of asphaltic hydrocarbon.

Pyrrhotite-rich massive sulfides (sample L1-16D-1) adjacent to a surficial barite crust have high Zn, Pb, Sb, and Ba, the highest Cu content (4.6 wt.%), and detectable Au (1.4 ppm). The barite crust (L1-16D-2) contains sphalerite and galena, but is nearly devoid of Cu-Fe sulfides. Concentrations of As, Ag, and Sb are higher than in the adjacent sulfide, whereas Bi and Se are lower. The barite crust also has a high Au value (2.0 ppm). Hannington *et al.* (1986) have also found a positive correlation between Au and Pb, Ag, As, and Sb in sulfides from Axial Seamount and southern Explorer Ridge.

The two polymetallic sulfide samples (dredge L2-14D) have very high Zn, Pb, As, Sb, Se, and Ag contents. Pb, As, and Sb concentrations of this magnitude have not been reported for bulk samples from any mid-ocean ridge. The sediment sample with a galena-rich sulfide matrix (L2-14D-6) has the highest Pb, As, Sb, and Sn, and lowest Cu of all the samples analyzed.

Sulfide wall

Chemical data for representative samples from the inner, middle, and outer sulfide wall of sample L2-

TABLE 3. BULK COMPOSITION OF MASSIVE SULFIDE, BARITE CRUST, AND SULFIDE-RICH SEDIMENT

	-----Pyrrhotite-rich sulfide-----				L1-16D-1	Barite crust L1-16D-2	Polymetallic sulfide		Sulfide-rich sediment	
	L1-24D-1	L2-180	L2-250	L6-32D-2			L2-14D-1	L2-14D-2	L2-14D-6	L2-14D-6
wt%										
As	0.03	0.55	N	0.50	0.20	0.72	1.70	2.70	2.75	
Ba	0.04	<0.005	<0.004	0.10	2.70	23.0	2.50	0.016	0.35	
Au	1.21	1.01	0.42	0.97	4.52	0.49	1.82	0.94	0.26	
Fe	42.0	35.2	57.0	40	33.3	6.4	33.1	16.9	22.9	
Pb	0.20	<0.02	<0.02	0.50	0.65	4.38	7.60	1.27	13.7	
Zn	0.34	0.07	1.10	1.60	2.30	17.3	20.3	43.2	7.10	
S	45.2	42.1	36.6	N	37.5	21.1	32.6	32.5	24.0	
C	0.32	0.13	0.11	5.6	0.14	0.15	0.07	0.06	2.24	
ppm										
Ag	14	<3	<3	40	67	2.0	681	184	339	
Au	<0.2	<0.2	<0.2	N	1.4	38.0	<0.2	<0.2	<0.2	
Bi	25	27	12	N	44	1.9	40	100	9.7	
Cd	4.4	4.8	4.5	50	270	830	630	1850	150	
Mn	100	7	7	3000	50	500	15	50	7000	
Sb	24	132	172	N	530	2700	960	1000	8700	
Se	180	380	380	200	95	<10	1000	720	<10	
Sn	300	500	200	500	70	150	700	700	>1500	

Analysts: R. Mays, J. Consul, C. Heropoulos, N. Elsheimer, J. Kent, S. Neil, P. LaMothe. Additional chemical data are reported in Benninger & Koski (1987).
N = Not analyzed

14D-1 are given in Table 4, and shown in Figure 10. As, Cu, Zn, Cd, and Se decrease outward from the inner wall; Pb, Ag, Sb, and Ba increase outward. The steepest gradients occur between the middle and outer wall. Sn and Hg are present at low levels in the inner and middle walls, but are also significantly enriched in the outer wall (Table 4).

MICROANALYSIS OF Fe-As-S PHASES

The textural characteristics of arsenopyrite and löllingite are illustrated in the BSE images of Figure 11. All EM analyses are plotted in the Fe-As-S ternary diagram of Figure 12; selected analyses are given in Table 5.

In the polymetallic massive sulfides (Figs. 11a,b), arsenopyrite grains commonly have narrow rims of löllingite. Figure 11a shows a grain with an arsenopyrite core (points 1-3) and a sawtooth margin of löllingite (points 4-6). The zigzag boundary between the two phases is distinct, but the pronounced streaking in the core and rim indicates that löllingite and arsenopyrite are intergrown on a very fine scale. Figure 11b shows rhombic Fe-As-S grains with narrow löllingite rims (point 9). The grain interiors have ribs of löllingite, but otherwise consist of homogeneous arsenopyrite (points 7, 8).

Fe-As-S grains from the middle wall of the sulfide structure are illustrated in Figures 11c-f. Along the boundary between the inner and middle walls, pyrrhotite is replaced by coarse-grained, homogeneous arsenopyrite (Fig. 11c, points 10-12). By contrast, the central part of the middle wall contains fine-grained arsenopyrite that is partly replaced by löllingite (Fig. 11d, points 13-17 and Fig. 11e, points 18-21).

In the outer part of the middle wall, the Fe-As-S phases typically form fine-grained rhombic crystals (Fig. 11f). Reverse zoning is present, with arsenopyrite rims (point 22) on dense clusters of very fine-grained, intermixed arsenopyrite and löllingite (points 23-25).

Analytical data for löllingite (points 26-30) in a pyrrhotite-rich sulfide sample (L6-32D-10) indicate that S contents exceed stoichiometric proportions. In addition, Co values of up to 2% indicate limited substitution for Fe in the $\text{CoAs}_2\text{-FeAs}_2$ solid-solution series.

The data plotted in Figure 12 span a near-continuum along the FeAsS-FeAs_2 join. The arsenopyrites have As enrichments similar to other naturally occurring arsenopyrites that coexist with pyrrhotite in sulfide deposits (Kretschmar & Scott 1976). The Fe enrichment of the Escanaba arsenopyrite grains (0.5 to 1.5 at.%) is, however, opposite to the Fe-depleted nature of many natural arsenopyrite samples (Kretschmar & Scott 1976, Sharp *et al.* 1985). Points that plot between

TABLE 4. BULK COMPOSITION OF INNER, MIDDLE, AND OUTER WALL OF POLYMETALLIC SULFIDE STRUCTURE, SAMPLE L2-14D-1

	Inner Wall	Middle Wall	Outer Wall
Wt%			
As	5.40	1.76	1.00
Cu	4.64	1.62	0.24
Fe	21.0	29.3	21.2
Pb	1.40	2.30	20.7
Zn	35.1	26.1	22.5
S	31.7	33.7	28.6
ppm			
Ag	150	200	3000
Ba	150	200	1500
Bi	95	88	73
Cd	1800	940	76
Hg	<2	<2	127
Mn	50	15	15
Sb	480	550	16,000
Se	1400	500	400
Sn	70	70	>1500

Additional analytical data are presented in Benninger & Koski (1987)

arsenopyrite and löllingite in Figure 12 probably represent analyses of finely intergrown mixtures of these phases that were unresolvable with the electron beam of the microprobe.

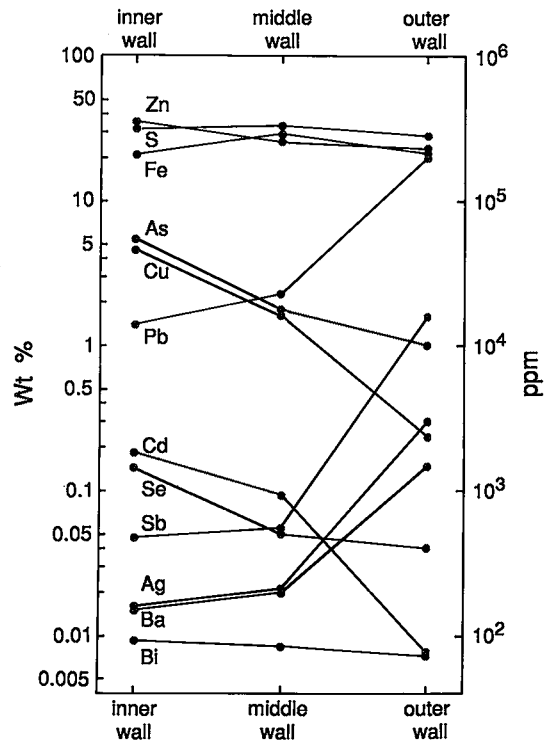


FIG. 10. Chemical variations across the wall of the polymetallic sulfide structure (sample L2-14D-1). The inner wall is inferred to have been in direct contact with hydrothermal fluid, whereas the outer wall was in contact with seawater.

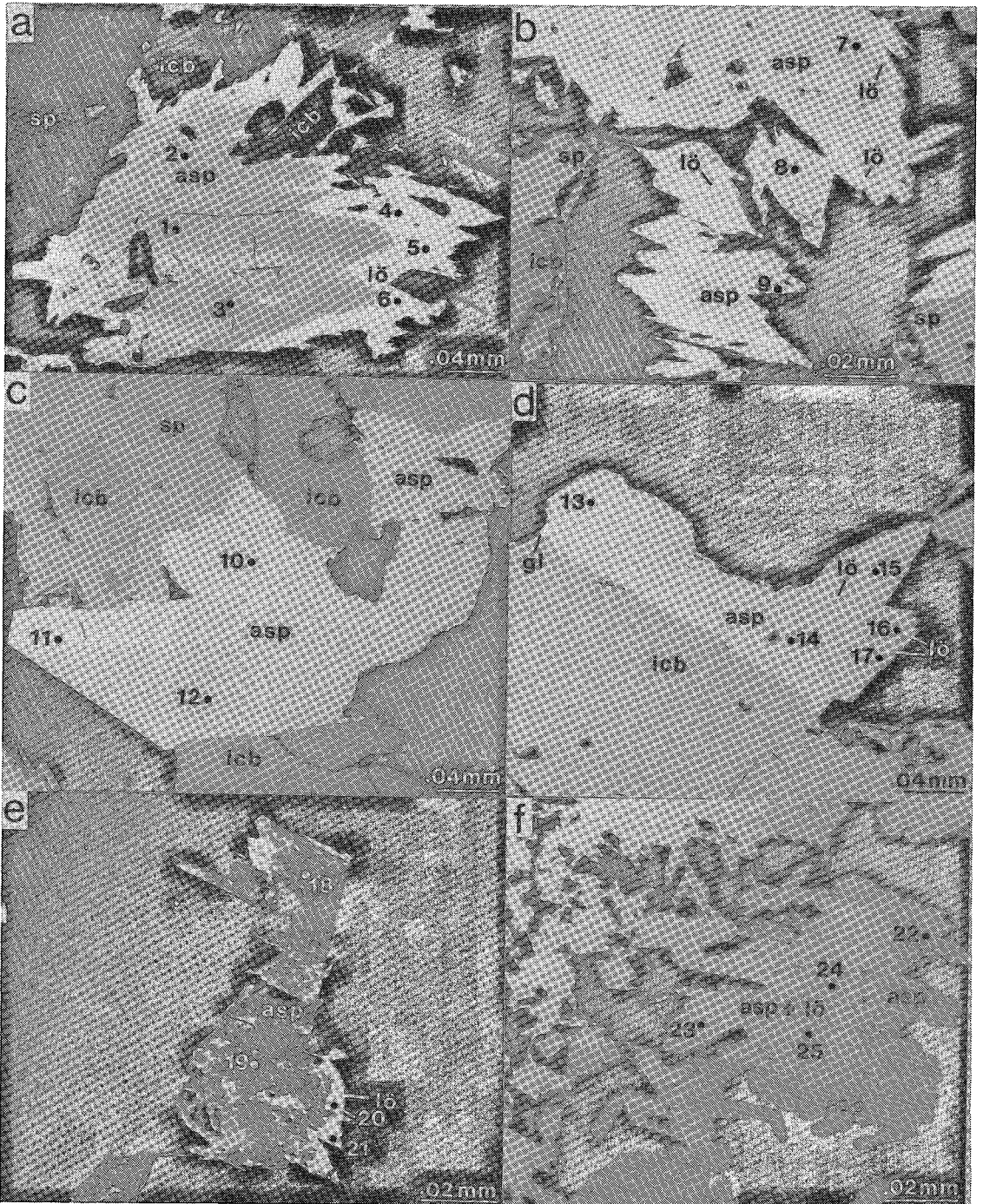


FIG. 11. BSE images of arsenopyrite (asp) and löllingite (lō) from polymetallic sulfide fragments, dredge L2-14D. Grains shown in images c through f are from the middle wall of sample L2-14D-1. The numbers (1–25) refer to electron-microprobe analysis points keyed to analyses in Table 5. Other phases are sphalerite (sp), isocubanite (icb), and galena (gl). (a) Anhedronal arsenopyrite grain with marginal replacement by löllingite; (b) rhombic arsenopyrite grains with thin rims and ribs of löllingite; (c) large homogeneous arsenopyrite grain near boundary with inner wall; (d) arsenopyrite with limited patchy replacement by löllingite; (e) arsenopyrite with advanced replacement by löllingite; (f) fine-grained aggregate with zoning in reverse of general relationship, that is, the core is a mixture of arsenopyrite + löllingite and the margin has arsenopyrite composition.

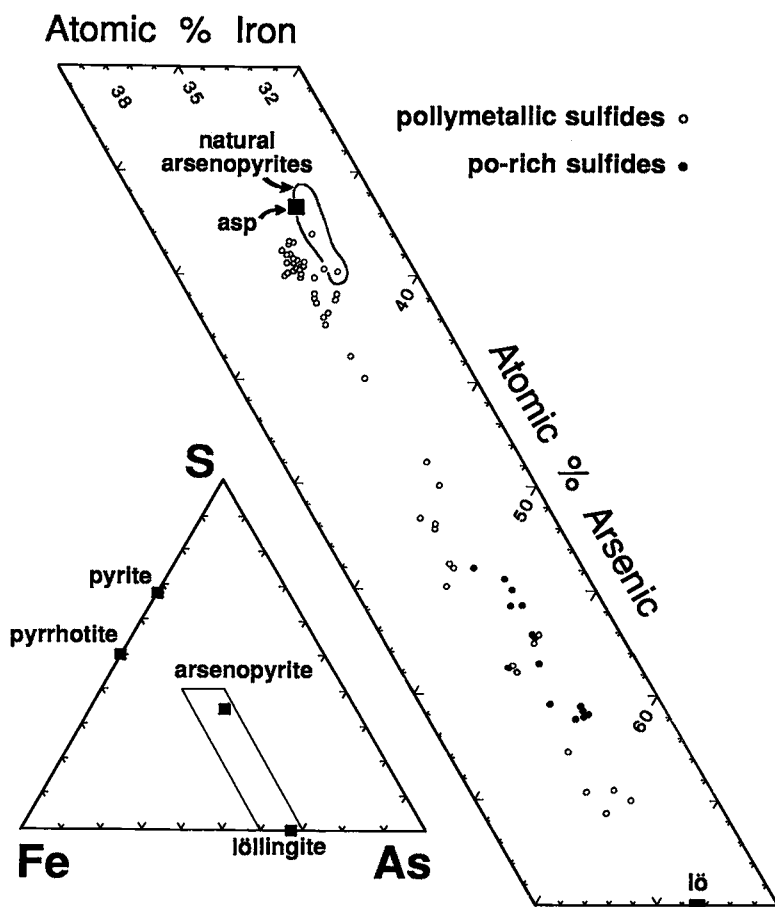


FIG. 12. Electron-microprobe analyses for arsenopyrite and löllingite from poly-metallic sulfides (L2-14D-1,2,4) and pyrrhotite-rich sulfides (L6-32D-10) plotted on Fe-As-S diagram. Arsenopyrite analyses are rich in Fe and As relative to stoichiometric FeAsS. The range in composition along the FeAsS-FeAs₂ join may result from analyses of fine-grained mixtures of the two phases. The field of natural arsenopyrites is from Kretschmar & Scott (1976).

SULFUR ISOTOPES

Preliminary sulfur isotope results for pyrrhotite and marcasite from hydrothermal deposits in the ET are given in Table 6 and are summarized in Figure 13. In all samples, pyrrhotite is the primary Fe sulfide; it is partly to completely replaced by marcasite. The $\delta^{34}\text{S}$ values for pyrrhotite have a wide range between 1.9 and 11.6‰ and average 6.6‰. The $\delta^{34}\text{S}$ values for marcasite range between 2.3 and 8.8‰ and have a lighter average of 5.2‰. Values for pyrrhotite in several samples from dredge L6-32D range between 5.3 and 11.6‰, generally higher than the two values for marcasite from the same dredge.

The $\delta^{34}\text{S}$ values for sulfides from sediment-starved ridge crests such as the East Pacific Rise at

21°N generally range between 1 and 4‰ and average about 2.5‰ (Styrt *et al.* 1981, Arnold & Shepard 1981, Kerridge *et al.* 1983, Zierenberg *et al.* 1984, Woodruff & Shanks 1988). These values result from the mixture of sulfide leached from basalt (0.3 ± 0.5 ‰, Sakai *et al.* 1984) and small amounts of sulfide derived from the quantitative reduction of seawater sulfate by Fe²⁺ in basalt (Shanks *et al.* 1981). Isotopic values heavier than about 4‰ for sulfides in chimneys and vent fluids are attributed either to entrainment of seawater by the discharging vent fluid or to replacement of sulfate phases by sulfides (Shanks & Seyfried 1987, Woodruff & Shanks 1988).

The range (1.9 to 11.6‰) and average (6.1‰) of $\delta^{34}\text{S}$ in ET sulfides indicate a proportionally

TABLE 5. ELECTRON MICROPROBE DATA FOR FE-AS-S MINERALS. ASP = ARSENOPYRITE, LO = LOLLINGITE

Analysis Point	Sample Number	Figure	Mineral	Weight Percent				Atomic Percent			Atomic Percent					
				Fe	Co	Ni	S	As	Sb	Total	Fe	Co	Ni	S	As	Sb
1	L2-14D-4	11a	asp	34.66	0.01	0.15	17.39	45.56	NA	97.77	34.99	0.01	0.14	30.58	34.28	--
2	"	11a	asp	34.16	0.01	0.15	16.28	47.86	NA	98.46	34.74	0.01	0.14	29.83	36.28	--
3	"	11a	asp	34.86	0.01	0.13	17.78	45.91	NA	98.69	34.80	0.01	0.12	30.91	34.16	--
4	"	11a	lo	29.89	0.07	0.22	3.55	66.01	NA	99.74	34.94	0.08	0.24	7.23	57.51	--
5	"	11a	lo	29.55	0.06	0.21	2.62	66.89	NA	99.33	35.09	0.07	0.23	5.42	59.19	--
6	"	11a	lo	29.20	0.08	0.22	2.08	68.11	NA	99.69	34.81	0.08	0.26	4.32	60.53	--
7	L2-14D-2	11b	asp	34.59	0.12	0.13	17.67	46.54	NA	99.05	34.49	0.11	0.12	30.69	34.59	--
8	"	11b	asp	34.26	0.03	0.15	17.12	47.94	NA	99.50	34.26	0.02	0.14	29.83	35.74	--
9*	"	11b	lo	24.98	NA	NA	1.81	72.23	NA	99.02						
10	L2-14D-1	11c	asp	34.57	0.03	0.16	16.35	48.57	0.13	99.81	34.75	0.03	0.15	28.62	36.39	0.06
11	"	11c	asp	34.89	0.06	0.13	17.28	47.32	0.18	99.86	34.70	0.05	0.13	29.95	35.09	0.08
12	"	11c	asp	35.03	0.03	0.14	17.69	46.61	0.16	99.66	34.75	0.03	0.13	30.56	34.46	0.07
13	"	11d	asp	34.83	0.04	0.15	17.05	45.81	0.11	97.99	35.21	0.04	0.15	30.02	34.53	0.05
14	"	11d	asp	33.32	0.03	0.12	16.22	48.87	0.11	98.67	33.93	0.03	0.12	28.78	37.09	0.05
15	"	11d	asp	34.14	0.04	0.15	15.42	48.84	0.14	98.73	34.96	0.04	0.15	27.51	37.28	0.06
16	"	11d	lo	29.70	0.05	0.15	6.60	64.11	0.20	100.81	33.28	0.05	0.16	12.87	53.54	0.10
17	"	11d	lo	29.91	0.05	0.16	6.32	63.66	0.20	100.30	33.74	0.05	0.17	12.42	53.52	0.10
18	"	11e	asp	34.13	0.03	0.16	15.96	49.27	0.10	99.65	34.52	0.03	0.15	28.11	37.14	0.05
19	"	11e	asp	32.69	0.03	0.12	17.03	48.39	0.11	98.37	33.15	0.03	0.11	30.08	36.58	0.05
20	"	11e	lo	28.34	0.06	0.15	2.40	69.44	0.24	100.63	33.50	0.06	0.17	4.95	61.19	0.13
21	"	11e	lo	28.26	0.07	0.16	2.63	67.54	0.24	98.90	33.84	0.08	0.18	5.48	60.29	0.13
22	"	11f	asp	33.68	0.03	0.14	18.49	46.77	0.51	99.62	33.29	0.03	0.13	31.85	34.47	0.23
23	"	11f	lo	30.79	0.10	0.22	5.56	63.21	0.39	100.27	34.96	0.10	0.24	11.00	53.50	0.20
24	"	11f	asp+lo	32.03	0.08	0.17	9.36	57.35	0.38	98.99	35.01	0.08	0.18	17.81	46.73	0.19
25	"	11f	asp+lo	30.94	0.04	0.14	10.41	56.13	0.37	98.03	33.90	0.04	0.14	19.88	45.85	0.19
26	L6-32D-10	lo	29.26	0.61	0.20	6.42	62.24	0.21	98.94	33.37	0.66	0.22	12.74	52.90	0.11	
27	"	lo	27.91	1.07	0.18	4.37	64.64	0.33	98.50	32.82	1.19	0.21	8.95	56.65	0.18	
28	"	lo	29.60	0.74	0.18	4.71	63.92	NA	99.15	34.29	0.81	0.20	9.50	55.20	--	
29	"	lo	29.18	2.13	0.19	7.15	61.29	NA	99.94	32.59	2.25	0.20	13.92	51.04	--	
30	"	lo	28.41	2.12	0.21	4.53	65.42	NA	100.69	32.56	2.30	0.23	9.03	55.88	--	

NA = Not analyzed

* determined by energy dispersive microanalyzer on SEM

Samples L2-14D-1, 2, and 4 are polymetallic massive sulfide; sample L6-32D-10 is pyrrhotite-rich massive sulfide dredge from the SESCOA site in 1985

Analysts: W. Bohrsen, R. Koski, R. Oscarson

TABLE 6. $\delta^{34}\text{S}$ (IN PER MIL) FOR FE-SULFIDE PHASES IN PYRRHOTITE-RICH MASSIVE SULFIDES

Sample Number	$\delta^{34}\text{S}$	
	Po	Mc
L1-3D		3.5
-15D	1.9	
-16A	5.0	5.4
-16B	4.7	5.0
-22D	4.6	3.8
-24D-A		5.8
-24D		6.2
-24D	5.5	5.5
-24D	6.2	
-34D	3.8	2.3
L6-32D-2*	5.6	8.8
-32D-3	11.6	
-32D-10	11.0	
-32D-21A	6.6	5.1
-32D-21B	5.3	5.4
-32D-24	11.5	
-32D-x	9.7	

Po = pyrrhotite, Mc = marcasite

* Dredged from SESCOA site in 1985

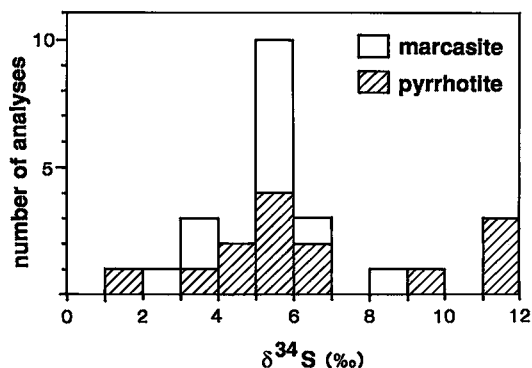
Analyst: W. C. Shanks

greater contribution of S from seawater sulfate. Sulfur isotope compositions highly enriched in ^{34}S are also reported for the sulfides at Middle Valley (Goodfellow *et al.* 1987). Immediate sources of sulfate at sediment-covered spreading axes include ambient seawater or seawater-dominated pore fluid at the discharge site, and earlier-formed sulfate phases in the hydrothermal mounds. A third source of sulfide, from reduction of sulfate within the sediment column, is discussed below. The absence of negative sulfur isotope values indicates that bacteriogenic sulfide is not an important contributor of sulfur in the ET hydrothermal system.

DISCUSSION

Hydrothermal circulation

The distribution and composition of massive sulfide deposits at the SESCOA and NESCA sites indicate circulation and widespread discharge of hydrothermal fluid through the sediment blanket of ET. The driving mechanism for fluid circulation is the buildup of heat within the volcanic basement owing to the insulating effect of the sediment blanket (Levi & Riddiough 1986). Although sulfur isotope data indicate a mixture of basaltic and seawater sulfate S in pyrrhotite-rich massive sulfides, the depth

FIG. 13. Histogram of $\delta^{34}\text{S}$ values (in per mil) for pyrrhotite and marcasite in pyrrhotite-rich massive sulfides.

of fluid penetration is unknown. Pb isotope ratios of pyrrhotite-rich and polymetallic massive sulfides from ET (LeHuray *et al.* 1988) are, however, nearly identical to values for turbidite in nearby DSDP Hole 35; no component of basaltic Pb is evident. Thus, hydrothermal fluids may penetrate the volcanic edifices in ET, but the composition of the massive sulfide deposits on the seafloor seems to be largely dependent on reactions between hydrothermal fluid and the sediment cover.

Within the sediment, heated fluids can migrate laterally through porous sand and silt turbidites. Mafic sills, volcanic flows, or clay horizons may provide suitable cap structures to guide the lateral movement of buoyant fluid (Lonsdale & Becker 1985). The hydrothermal fluids may be channeled to the surface along faults that bound the sediment-capped hills (Fig. 4) and step-faults that downdrop sediment on the northern flank of the volcanic hill at NESCA. Other deposits in the form of spires and sheets have formed from emanations between the hills and on the west flank of the lava lake at the NESCA site. Seawater recharge for the hydrothermal systems may take place by downwelling on the margins of the axial valley, but the most favorable recharge sites may be axis-parallel faults displacing sediment near the volcanic edifices, or antithetic structures associated with faults around the sediment-capped hills.

Fluid-sediment interaction

The high content of Pb and other metals in polymetallic sulfides, and the paucity of chalcophile metals (except Cu) in pyrrhotite-rich sulfides, indicate extensive interaction between hydrothermal fluid and sediment at depth. The mobilization of metals during interaction between hydrothermal fluid and sediment has been studied experimentally by Bischoff *et al.* (1981) and Thornton & Seyfried (1987). In the first study, greywacke was reacted with a saturated NaCl brine at 350°C, 500 bars, and a fluid/rock ratio of 10/1. The greywacke was partly altered to an assemblage of chlorite-smectite + albite. H⁺ ions were produced by Mg metasomatism, and significant quantities of metals (Zn, Ni, Cu, Pb, Sb, and Cd) were partitioned into the fluid. When greywacke was reacted with seawater (~0.5 *m* NaCl) under the same conditions, lower amounts of metals were solubilized; only Sb was released into solution in quantitative amounts. The seawater that reacted with greywacke acquired lower pH values than that observed in basalt-seawater experiments conducted under comparable conditions (Seyfried 1977).

Thornton & Seyfried (1987) reacted organic-rich diatomaceous sediment with seawater at 350°C, 500 bars, and a seawater/sediment ratio of 3/1. The reaction resulted in alteration of sediment to chlorite-smectite, and solubilization of metals (Fe, Cu, As,

Pb). The fluid acidity was controlled by competing inorganic and organic processes: production of H⁺ by Mg and Na fixation in secondary silicates, and consumption of H⁺ by the hydrothermal alteration of organic matter. Thornton & Seyfried (1987) also noted a time correspondence between Pb and acetate in solution, and suggested that Pb solubility may be enhanced by organo-metallic complexing.

The presence of aliphatic and aromatic hydrocarbons in pyrrhotite-rich sulfides at the SESCA site indicates rapid, high-temperature maturation of continentally-derived plant matter in the sediment (Kvenvolden *et al.* 1986). Interaction between hydrothermal fluid and the organic fraction of the sediment may also provide a mechanism for sulfate reduction that could explain the ³⁴S-enriched values for ET sulfides (Table 6). Thornton & Seyfried (1987) proposed that acetate produced by the hydrothermal decomposition of organic matter can reduce dissolved sulfate as shown in the reaction: CH₃COOH + SO₄²⁻ + 2H⁺ = 2H₂CO₃ + H₂S. Furthermore, acetate and ammonium produced by the thermal degradation of organic matter have a buffering effect on the hydrothermal fluid (Von Damm *et al.* 1985b, Thornton & Seyfried 1987) that may promote the subsurface deposition of sulfide minerals.

Deposition of pyrrhotite-rich sulfide

The rubbly, partly oxidized appearance of many pyrrhotite-rich massive sulfide samples dredged from the SESCA and NESCA sites suggests that much of this material is sulfide talus from rapidly eroded mounds constructed at the margins of sediment-capped hills. In our depositional model for pyrrhotite-rich sulfide (Fig. 14a), upwelling hydrothermal fluids follow throughgoing structures at depth (*e.g.*, bounding faults), before spreading out along subsidiary fault splays and antithetic structures that disrupt the sediment near the seafloor. Diffuse low-velocity discharge along these structures and through unconsolidated sediment on the seafloor results in increased subsurface mixing, decreased fluid temperatures, and enhanced subsurface deposition of sulfide.

The absence of mineral zonation within the pyrrhotite-rich deposits suggests that gentle temperature and chemical gradients prevailed during mound buildup at the discharge site. The textural heterogeneity of pyrrhotite, especially the occurrence of coarse-grained and radially oriented aggregates, is thought to result from flow through myriad fluid channelways within the deposit.

The sulfide paragenesis is consistent within all of the pyrrhotite-rich sulfide samples studied: early-formed pyrrhotite is followed by sphalerite and Cu-Fe sulfides, löllingite and native bismuth, and mar-

casite. Pyrrhotite stability may be enhanced by low sulfur and oxygen fugacities of the fluids. These conditions may reflect earlier seafloor deposition of chalcopyrite and pyrite at depth, and the oxidation of organic matter in the sediment. The partial replacement of pyrrhotite by sphalerite and Cu-Fe sulfides represents a prograde mineralization sequence involving fluids at progressively higher temperatures. This paragenesis is similar to that observed in massive sulfide deposits from Guaymas Basin (Koski *et al.* 1985, Peter 1986) and Middle Valley (Davis *et al.* 1987).

The layered aggregates of löllingite and native bismuth are superimposed on earlier-formed pyrrhotite, sphalerite, and Cu-Fe sulfides. The analyses of löllingite from pyrrhotite-rich sample L6-32D-10 (Table 5) indicate that löllingite grains contain some finely intergrown arsenopyrite that was not resolved during EM analysis. Phase equilibria in the Fe-As-S system show that the deposition of both löllingite and arsenopyrite would be favored by fluid with high As activity (Barton 1969). However, their individual stabilities are also dependent on the S_2 activity in the fluid according to the reaction: $2FeAs_2 + S_2 = 2FeAsS + 2As$. The restricted distribution of Fe-As-S phases and native bismuth around fluid channelways indicates that deposition occurred during intermittent discharge of As- and Bi-rich fluids. The occurrence of arsenopyrite-löllingite intergrowths may record fluctuations of the As/ S_2 ratio in the fluid.

In our model, chimneys atop the sulfide mounds vented hydrothermal fluid into the water column, but a considerable volume of fluid also diffused through the mound surface (Fig. 14a). This diffuse discharge and the subsequent mixing with sulfate-rich seawater resulted in the deposition of a barite-anhydrite crust over massive sulfide. Anhydrite is an abundant phase in actively forming deposits in Guaymas Basin (Lonsdale & Becker 1985, Peter 1986) but is absent from the ET samples, possibly because of its retrograde solubility in cold seawater. Though only a few cm in thickness, the sulfate crust had sufficient density to inhibit access of ambient seawater to the interior of the sulfide mound. An increase in temperature under the sulfate carapace resulted in the interstitial deposition of sphalerite and Cu-Fe sulfides. Sphalerite and galena were quenched as dendritic and colloform overgrowths on barite where fluids leaked through the sulfate carapace.

We interpret the crack-controlled and pseudomorphic replacement of pyrrhotite by "intermediate" alteration products (Einaudi 1971) and marcasite to be a consequence of "hydrothermal ageing" of massive sulfides, that is, the gradual oxidative alteration of earlier-formed sulfide phases as the redox potential of the hydrothermal fluid increased with time. Covellite and digenite may also have

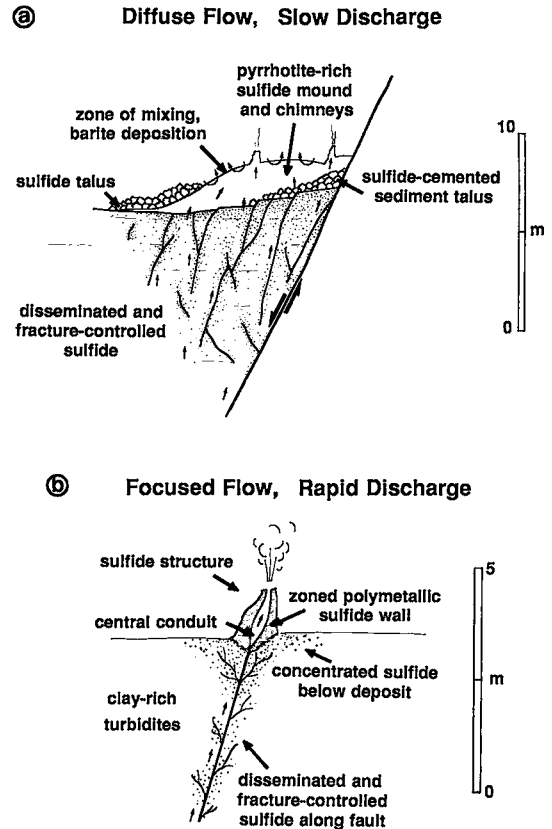


FIG. 14. Generalized models for formation of (a) a pyrrhotite-rich sulfide mound, and (b) the zoned polymetallic sulfide structure.

formed during this gradual alteration process.

Deposition of the polymetallic sulfide structure

Polymetallic sulfide samples seem to be derived from a zoned sulfide structure with a large central conduit. In the model proposed here, the mineral assemblage and telescoped zonation were formed in response to steep temperature and chemical gradients within the vent. Such gradients could have resulted from a focused, high-velocity discharge analogous to venting at "black smoker" vents on the EPR (Rise Group 1980, Macdonald *et al.* 1980). At the NESCA site, fluid may have discharged from a fault zone that crosscut impermeable clay-rich turbidites (Fig. 14b). Clay-rich sediment has been recovered from gravity cores of surficial sediment (Karlin & Lyle 1986), and clay and clayey silt layers occur within the upper 50 m of the sediment section cored at DSDP Site 35 in ET (Vallier *et al.* 1973). The focused upwelling of the hydrothermal fluid prevented large-scale sub-

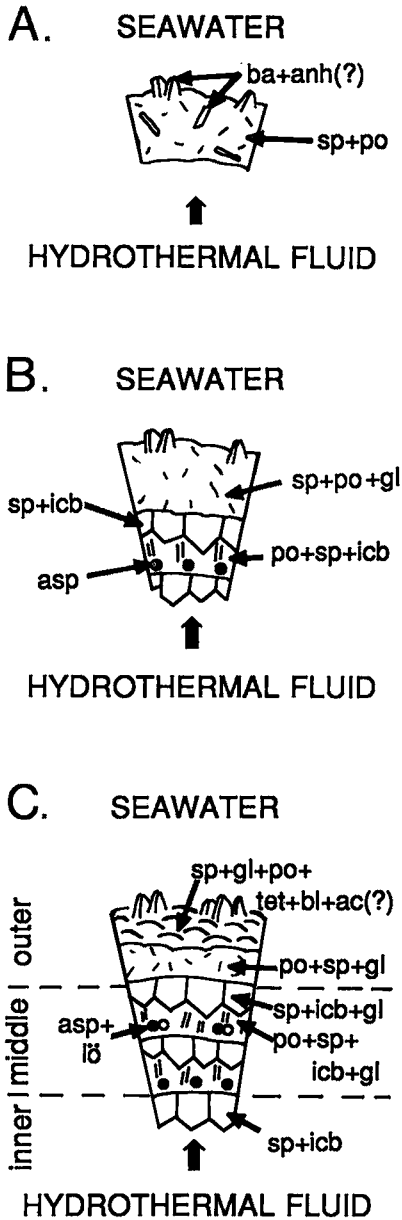


FIG. 15. Growth of polymetallic sulfide wall and development of sulfide-sulfate zonation. (A) Formation of early-formed sulfide-sulfate wall composed of sphalerite (sp), pyrrhotite (po), barite (ba), and probably, anhydrite (anh). (B) Deposition at higher temperature of alternating layers of sphalerite + isocubanite (icb) and subparallel pyrrhotite (+ sphalerite + isocubanite) inside the sulfide-sulfate shell. Arsenopyrite (asp) is deposited in the pyrrhotite-rich layer, and galena (gl), as well as additional sphalerite and sulfate phases, is deposited on the outer surface. (C) Sulfide wall thickens by inward deposition of additional sphalerite + isocubanite and pyrrhotite-rich layers and outward

surface deposition of metals, and thus preserved the initial metal-rich composition of the fluid. The galena-rich sediment sample (L2-14D-6) recovered at this site may represent subsurface mineralization near the fluid channelway.

The mineral zonation and texture in the polymetallic sulfide wall indicate a complex growth history for the sulfide structure within an intensifying hydrothermal system. In our interpretation, the original wall of the sulfide structure, consisting of sphalerite, pyrrhotite, barite, and probably anhydrite, precipitated at relatively low temperature at the mixing interface between hydrothermal fluid and seawater (Fig. 15a). Pyrrhotite crystallized in random orientation, whereas sphalerite and barite grew outward as dendrites into seawater. Anhydrite, an important component in the construction of black-smoker chimneys on the EPR (Haymon 1983), was probably deposited in the polymetallic sulfide structure, but subsequently dissolved in cold seawater.

As venting and construction of the sulfide structure continued, alternating layers of sphalerite + isocubanite and layers of subparallel pyrrhotite tablets developed inward from, and partly replaced, the sulfide-sulfate shell (Figs. 15b,c). In this higher temperature milieu, each layer of sphalerite + isocubanite (except the inner-wall assemblage) formed earlier than, and was partly replaced by, the more interior pyrrhotite-rich layer. Sharp contacts between layers indicate rapid variations in fluid temperature and (or) composition (e.g., metal content and sulfur fugacity). Sphalerite and isocubanite of the inner wall represent the last stage of high-temperature sulfide deposition. Isocubanite replaced the Fe-rich parts of sphalerite grains to produce skeletal textures and chalcopyrite disease.

The episodic deposition of arsenopyrite and zoned arsenopyrite-löllingite aggregates occurred at high temperature within the pyrrhotite-rich layers of the middle wall. Arsenopyrite replaced pyrrhotite, sphalerite + and isocubanite and was partly replaced by löllingite when As/S₂ ratios in the fluids increased.

During continued leakage of hydrothermal fluid through the sulfide structure, a fine-grained assemblage of sphalerite, galena, pyrrhotite, barite, boulangerite, tetrahedrite, and Ag sulfide (acanthite?) was quenched on the outer wall (Fig. 15c). The zone of galena deposition also migrated into the middle wall as the inward precipitation of multiple

growth of the fine-grained assemblage sphalerite + galena + pyrrhotite + tetrahedrite (tet) + boulangerite (bl) + Ag sulfide (possibly acanthite, ac). Arsenopyrite is deposited in the innermost pyrrhotite-rich layer, and earlier-formed arsenopyrite is partly replaced by löllingite (lö). Galena is deposited in the middle wall as the sulfide wall expands.

layers of sphalerite + isocubanite and pyrrhotite thickened the sulfide structure.

CONCLUSIONS

The composition, sulfur isotope data, and petroleum content of sulfide deposits in ET reflect extensive interaction between hydrothermal fluid and turbiditic sediment. Nearly monomineralic, pyrrhotite-rich sulfide samples with thin Au-bearing barite crusts are fragments of rapidly eroded hydrothermal mounds. The mounds formed within a diffuse, low-velocity flow regime with minimal temperature and chemical gradients. Grain-size heterogeneity within individual samples represents myriad fluid channelways in the sulfide mounds. Subsurface deposition of chalcopyrite and pyrite, and interaction between fluid and organic matter, may account for the pyrrhotite-rich nature of the sulfide.

Polymetallic massive sulfide fragments are from a zoned sulfide structure with a large central conduit. Telescoped mineralogical and chemical zonations reflect steep temperature and chemical gradients at a site of focused, high-velocity fluid discharge, possibly above a fault that disrupted clay-rich turbiditic sediment. Following deposition of an early low-temperature sulfide-sulfate shell, the high-temperature assemblage sphalerite + isocubanite + pyrrhotite grew inward toward the hydrothermal fluid, whereas the low-temperature assemblage galena + sphalerite + pyrrhotite + barite + boulangerite + tetrahedrite + Ag sulfide (acanthite?) grew outward from the outer wall as hydrothermal fluid leaked through the sulfide structure and mixed with ambient seawater. Galena, arsenopyrite, and löllingite were deposited in the middle wall as the sulfide wall increased in thickness.

ACKNOWLEDGEMENTS

The results represent a collective effort by many colleagues at the U.S. Geological Survey. Janet Morton, William Normark, Mark Holmes, and David Clague served as Chief Scientists during several cruises to the Gorda Ridge. The samples could not have been collected without the nautical expertise of Captain Allan McClenaghan and the crew of the U.S. Research Vessel *S.P. LEE*. Careful reviews by David Clague, Robert Rosenbauer, Ian Jonasson, and an anonymous reviewer are appreciated. An especially detailed review by Tim Barrett was particularly helpful. We are grateful for the drafting expertise of Laura Benninger and patient handling of the manuscript by Kay Beecher and Lisa Gein.

REFERENCES

ABBOTT, D.H., MORTON, J.L. & HOLMES, M.L. (1986):

Heat-flow measurements on a hydrothermally-active, slow-spreading ridge: the Escanaba Trough. *Geophys. Res. Lett.* **13**, 678-680.

- ALBEE, A.L. & RAY, L. (1970): Correction factors for electron probe analysis of silicates, oxides, carbonates, phosphates, and sulfates. *Anal. Chem.* **42**, 1408-1414.
- ARNOLD, M. & SHEPPARD, M.F. (1981): East Pacific Rise at latitude 21°N: isotopic composition and origin of the hydrothermal sulphur. *Earth Planet. Sci. Lett.* **56**, 148-156.
- ATWATER, T. & MUDIE, J.D. (1973): Detailed near-bottom geophysical study of the Gorda Rise. *J. Geophys. Res.* **78**, 8665-8686.
- BÄCKER, H. & LANGE, J. (1987): Recent hydrothermal metal accumulation, products, and conditions of formation. In *Marine Minerals—Advances in Research and Resource Assessment* (P.G. Teleki, M.R. Dobson, *et al.*, eds.). D. Reidel Publ. Co., Dordrecht, Holland.
- BARTON, P.B., JR. (1969): Thermochemical study of the system Fe-As-S. *Geochim. Cosmochim. Acta* **33**, 841-857.
- _____ (1978): Some ore textures involving sphalerite from the Furutobe mine, Akita Prefecture, Japan. *Mining Geol.* **28**, 293-300.
- _____ & BETHKE, P.M. (1987): Chalcopyrite disease in sphalerite: Pathology and epidemiology. *Amer. Mineral.* **72**, 451-467.
- BENNINGER, L.M. & KOSKI, R.A. (1987): Descriptions of sulfide samples dredged in 1986 from Escanaba Trough, southern Gorda Ridge. *U.S. Geol. Surv. Open-File Rep.* **87-375-B**.
- BIBEE, L.D. (1986): Ocean bottom seismometer measurements on the Gorda Ridge. *Oregon Dep. Geol. Mineral Indust. Open-File Rep.* **0-86-15**.
- BISCHOFF, J.L., RADKE, A.S. & ROSENBAUER, R.J. (1981): Hydrothermal alteration of graywacke by brine and seawater: Roles of alteration and chloride complexing on metal solubilization at 200° and 350°C. *Econ. Geol.* **76**, 659-676.
- _____, ROSENBAUER, R.J., ARUSCAVAGE, P.J., BAEDCKER, P.A. & CROCK, J.G. (1983): Sea-floor massive sulfide deposits from 21°N, East Pacific Rise; Juan de Fuca Ridge; and Galapagos Rift: Bulk chemical composition and economic implications. *Econ. Geol.* **78**, 1711-1720.
- BREVART, O., DUPRE, B. & ALLEGRE, C.J. (1981): Metallogenesis at spreading centers: Lead isotope systematics for sulfides, manganese-rich crusts, basalts, and sediments from the Cyamex and Alvin areas (East Pacific Rise). *Econ. Geol.* **76**, 1205-1210.
- CANFIELD, D.E., RAISWELL, R., WESTRICH, J.T., REAVES, C.M. & BERNER, R.A. (1986): The use of chromium reduction in the analysis of reduced inorganic sulfur in sediments and shales. *Chem. Geol.* **54**, 149-155.
- CHEN, J.H., WASSERBURG, G.J., VON DAMM, K.L. & EDMOND, J.M. (1986): The U-Th-Pb systematics in hot springs on the East Pacific Rise at 21°N and Guaymas Basin. *Geochim. Cosmochim. Acta* **50**, 2467-2479.
- DAVIS, E.E., GOODFELLOW, W.D., BORNHOLD, B.D., ADSHEAD, J., BLAISE, B., VILLINGER, H. & LE

- CHEMINANT, G.M. (1987): Massive sulfides in a sedimented rift valley, northern Juan de Fuca Ridge. *Earth Planet. Sci. Lett.* **82**, 49-61.
- EINAUDI, M.T. (1971): The intermediate product of pyrrhotite alteration. *Amer. Mineral.* **56**, 1297-1302.
- GOODFELLOW, W.D., JONASSON, I.R., BLAISE, B., FRANKLIN, J.M. & GRAPES, K. (1987): Nature of sulfide-rich mounds in sediment-filled Middle Valley, northern Juan de Fuca Ridge. *EOS, Trans. Amer. Geophys. Union* **68**, 1546.
- HANNINGTON, M.D., PETER, J.M. & SCOTT, S.D. (1986): Gold in sea-floor polymetallic sulfide deposits. *Econ. Geol.* **81**, 1867-1883.
- HAYMON, R.L. (1983): The growth history of hydrothermal black smoker chimneys. *Nature* **301**, 695-698.
- HÉKINIEN, R., FEVRIER, M., BISCHOFF, J.L., PICOT, P. & SHANKS, W.C., III (1980): Sulfide deposits from the East Pacific Rise near 21°N. *Science* **207**, 1433-1444.
- _____, & FOUQUET, Y. (1985): Volcanism and metallogenesis of axial and off-axial structures on the East Pacific Rise near 13°N. *Econ. Geol.* **80**, 221-249.
- HOLMES, M.L. & ZIERENBERG, R.A. (1988): Submersible observations in Escanaba Trough, southern Gorda Ridge. In *The Gorda Ridge: a Frontier Area in the United States Exclusive Economic Zone* (G. R. McMurray, ed.). Proc. of the Gorda Ridge Symp., May 11-13, 1987, Portland, Oregon (in press).
- JAMBOR, J.L. (1967): New lead sulfantimonides from Madoc, Ontario. Part 2, mineral descriptions. *Can. Mineral.* **9**, 191-213.
- KARLIN, R. & LYLE, M. (1986): Sediment studies on the Gorda Ridge. *Oregon Dep. Geol. Mineral Indust. Open-File Rep.* **0-86-19**.
- KERRIDGE, J.F., HAYMON, R.M. & KASTNER, M. (1983): Sulfur isotope systematics at the 21°N site, East Pacific Rise. *Earth Planet. Sci. Lett.* **66**, 91-100.
- KOSKI, R.A., LONSDALE, P.F., SHANKS, W.C., III, BERNDT, M.E. & HOWE, S.S. (1985): Mineralogy and geochemistry of a sediment-hosted hydrothermal sulfide deposit from the Southern Trough of Guaymas Basin, Gulf of California. *J. Geophys. Res.* **90**, 6695-6707.
- _____, ZIERENBERG, R.A., KVENVOLDEN, K.A. & SHANKS, W.C., III (1987): Mineralogy and chemistry of hydrothermal sulfide and petroleum deposits from Escanaba Trough, Gorda Ridge. *U.S. Geol. Surv. Circ.* **995** (abstr.).
- KRETSCHMAR, U. & SCOTT, S.D. (1976): Phase relations involving arsenopyrite in the system Fe-As-S and their application. *Can. Mineral.* **14**, 364-386.
- KVENVOLDEN, K.A., RAPP, J.B., HOSTETTLER, F.D., MORTON, J.L., KING, J.D. & CLAYPOOL, G.E. (1986): Petroleum associated with polymetallic sulfide in sediment from Gorda Ridge. *Science* **234**, 1231-1234.
- LEHURAY, A.P., CHURCH, S.E., KOSKI, R.A. & BOUSE, R.M. (1988): Pb isotope ratios in sulfides from mid-ocean ridge hydrothermal sites. *Geology* **16**, 362-365.
- LEVI, S. & RIDDIHOUGH, R. (1986): Why are marine magnetic anomalies suppressed over sedimented spreading centers?. *Geology* **14**, 651-654.
- LONSDALE, P. & BECKER, K. (1985): Hydrothermal plumes, hot springs, and conductive heat flow in the Southern Trough of Guaymas Basin. *Earth Planet. Sci. Lett.* **73**, 211-225.
- LONSDALE, P.F., BISCHOFF, J.L., BURNS, V.M., KASTNER, M. & SWEENEY, R.E. (1980): A high-temperature hydrothermal deposit on the seabed at a Gulf of California spreading center. *Earth Planet. Sci. Lett.* **49**, 8-20.
- LUPTON, J.E. (1983): Fluxes of helium-3 and heat from submarine hydrothermal systems: Guaymas Basin versus 21°N, EPR. *EOS, Trans. Amer. Geophys. Union* **64**, 723.
- MACDONALD, K.C., BECKER, K., SPIESS, F.N. & BALLARD, R.D. (1980): Hydrothermal heat flux of the "black smoker" vents on the East Pacific Rise. *Earth Planet. Sci. Lett.* **48**, 1-7.
- MORTON, J.L., HOLMES, M.L. & KOSKI, R.A. (1987a): Volcanism and massive sulfide formation at a sedimented spreading center, Escanaba Trough, Gorda Ridge, northeast Pacific Ocean. *Geophys. Res. Lett.* **14**, 769-772.
- _____, NORMARK, W.R., ROSS, S.L., KOSKI, R.A., HOLMES, M.L., SHANKS, W.C., III, ZIERENBERG, R.A., LYLE, M. & BENNINGER, L.M. (1987b): Preliminary report, cruises L1-86-NC and L2-86-NC, Escanaba Trough, Gorda Ridge. *U.S. Geol. Surv. Open-File Rep.* **87-375-A**.
- MUROWCHICK, J.B. & BARNES, H.L. (1984): The recognition and significance of porous pyrite. *Geol. Soc. Amer. Program Abstr.* **16**, 604.
- _____, & _____ (1986): Marcasite precipitation from hydrothermal solutions. *Geochim. Cosmochim. Acta* **50**, 2615-2629.
- PETER, J.M. (1986): *Genesis of Hydrothermal Vent Deposits in the Southern Trough of Guaymas Basin, Gulf of California: a Mineralogical and Geochemical Study*. M.S. thesis, Univ. Toronto, Toronto, Ontario.
- REES, C.E. (1978): Sulphur isotope measurements using SO₂ and SF₆. *Geochim. Cosmochim. Acta* **42**, 383-389.
- RIDDIHOUGH, R.P. (1980): Gorda Plate motions from magnetic anomaly analysis. *Earth Planet. Sci. Lett.* **51**, 163-170.
- RISE GROUP (1980): East Pacific Rise: hot springs and geophysical experiments. *Science* **207**, 1421-1433.
- SAKAI, H., DES MARAIS, D.J., UEDA, A. & MOORE, J.G. (1984): Concentrations and isotope ratios of carbon, nitrogen and sulfur in ocean-floor basalts. *Geochim. Cosmochim. Acta* **48**, 2433-2441.
- SEYFRIED, W.E. (1977): *Seawater-Basalt Interaction from 25°C to 350°C and 1-500 Bars*. Ph.D. thesis, Univ. South. California, Los Angeles, California.
- SHANKS W.C., III & NIEMITZ, J. (1982): Sulfur isotope studies of hydrothermal anhydrite and pyrite. *Initial Reports Deep Sea Drilling Project* **64**, 1137-1142. U.S. Gov. Printing Office, Washington, D.C.
- _____, & SEYFRIED, W.E. (1987): Stable isotope studies of vent fluids and chimney minerals, southern Juan de Fuca Ridge: Sodium metasomatism and seawater sulfate reduction. *J. Geophys. Res.* **92**, 11387-11399.
- _____, BISCHOFF, J.L. & ROSENBAUER, R.J., (1981): Seawater sulfate reduction and sulfur isotope fractionation in basaltic systems: Interaction of seawater with fayalite and magnetite at 200-350°C. *Geochim.*

- Cosmochim. Acta* **45**, 1977-1995.
- SHARP, Z.D., ESSENE, E.J. & KELLY, W.C. (1985): A re-examination of the arsenopyrite geothermometer: pressure considerations and applications to natural assemblages. *Can. Mineral.* **23**, 517-534.
- SIMONEIT, B.R.T. (1985): Hydrothermal petroleum: genesis, migration, and deposition in Guaymas Basin, Gulf of California. *Earth Planet. Sci. Lett.* **22**, 1919-1929.
- _____, & LONSDALE, P.F. (1982): Hydrothermal petroleum in mineralized mounds at the seabed of Guaymas Basin. *Nature* **295**, 198-202.
- STYRT, M.M., BRACKMANN, A.J., HOLLAND, H.D., CLARK, B.C., PISUTHA-ARNOND, V., ELDRIDGE, C.S. & OHMOTO, H. (1981): The mineralogy and the isotopic composition of sulphur in hydrothermal sulphide/sulphate deposits on the East Pacific Rise, 21°N latitude. *Earth Planet. Sci. Lett.* **53**, 382-390.
- THORNTON, E.C. & SEYFRIED, W.E., JR. (1987): Reactivity of organic-rich sediment in seawater at 350°C, 500 bars: Experimental and theoretical constraints and implications for the Guaymas Basin hydrothermal system. *Geochim. Cosmochim. Acta* **51**, 1997-2010.
- VALLIER, T.L., HARROLD, P.J. & GIRDLEY, W.A. (1973): Provenances and dispersal patterns of turbidite sand in Escanaba Trough, northeastern Pacific Ocean. *Marine Geol.* **15**, 67-87.
- VIDAL, PH. & CLAUER, N. (1981): Pb and Sr isotopic systematics of some basalts and sulfides from the East Pacific Rise at 21°N (Project RITA). *Earth Planet. Sci. Lett.* **55**, 237-246.
- VON DAMM, K.L. & BISCHOFF, J.L. (1987): Chemistry of hydrothermal solutions from the southern Juan de Fuca Ridge. *Geochim. Cosmochim. Acta* **92**, 11334-11346.
- _____, EDMOND, J.M., GRANT, B., MEASURES, C.I., WALDEN, B. & WEISS, R.F. (1985a): Chemistry of submarine hydrothermal solutions at 21°N, East Pacific Rise. *Geochim. Cosmochim. Acta* **49**, 2197-2220.
- _____, _____, MEASURES, C.I. & GRANT, B. (1985b): Chemistry of submarine hydrothermal solutions at Guaymas Basin, Gulf of California. *Geochim. Cosmochim. Acta* **49**, 2221-2237.
- WOODRUFF, L.G. & SHANKS, W.C., III (1988): Sulfur isotope study of chimney minerals and vent fluids from 21°N, East Pacific Rise: Hydrothermal sulfur sources and disequilibrium sulfate reduction. *J. Geophys. Res.* **93**, 4562-4572.
- ZIERENBERG, R.A., SHANKS, W.C., III & BISCHOFF, J.L. (1984): Massive sulfide deposits at 21°N, East Pacific Rise: Chemical composition, stable isotopes, and phase equilibria. *Geol. Soc. Amer. Bull.* **95**, 922-929.

Received September 30, 1987; revised manuscript accepted May 28, 1988.